Real-Time Motor Unit Identification From High-Density Surface EMG

Vojko Glaser, Aleš Holobar, *Member, IEEE*, and Damjan Zazula, *Senior Member, IEEE*

***Abstract*—This study addresses online decomposition of high-density surface electromyograms (EMG) in real time. The proposed method is based on the previously published Convolution Kernel Compensation (CKC) technique and shares the same decomposition paradigm, i.e., compensation of motor unit action potentials and direct identification of motor unit (MU) discharges. In contrast to previously published version of CKC, which operates in batch mode and requires ∼10 s of EMG signal, the real-time implementation begins with batch processing of ∼3 s of the EMG signal in the initialization stage and continues on with iterative updating of the estimators of MU discharges as blocks of new EMG samples become available. Its detailed comparison to previously validated batch version of CKC and asymptotically Bayesian optimal linear minimum mean square error (LMMSE) estimator demonstrates high agreement in identified MU discharges among all three techniques. In the case of synthetic surface EMG with 20 dB signal-to-noise ratio, MU discharges were identified with average sensitivity of 98%. In the case of experimental EMG, real-time CKC fully converged after initial 5 s of EMG recordings and real-time and batch CKC agreed on 90% of MU discharges, on average. The real-time CKC identified slightly fewer MUs than its batch version (experimental EMG, 4 MUs versus 5 MUs identified by batch CKC, on average), but required only 0.6 s of processing time on regular personal computer for each second of multichannel surface EMG.**

***Index Terms*—Discharge pattern, high-density electromyograms (EMG), motor unit, real-time decomposition, surface EMG.**

I. Introduction

In the last decade, decomposition of electromyograms (EMG) into individual motor unit action potential (MUAP) trains gathered considerable interest in neurophysiological and clinical communities, as it enables reliable and robust quantification of neural drive to muscles [8]. Among the others, EMG decomposition algorithms have been successfully applied in neurophysiological investigations of healthy subjects [1], [7], [23], [25] and [33], patients with pathological tremor [20], cramps [30] and other neuromuscular disorders [9] and [35].

Various techniques for EMG decomposition have been proposed, ranging from template matching applied to indwelling [27], [31] and surface EMG [11], [25], [32], to higher order statistics [37], and to blind source separation of high-density EMG [15]. Among them, the analyses of multichannel indwelling EMG [6] and noninvasively acquired surface EMG [15], [32] have demonstrated the most remarkable progress. The first one enables sampling from a large number of motor units (MUs), guaranteeing the representativeness of results in neurophysiological and pathophysiological studies. The second one supports frequent and long-term MU tracking also outside the clinical environment as the acquisition of surface EMG signals is relatively simple and presents no significant risk. The latter makes surface EMG an appealing candidate also for objective assessments of rehabilitation techniques, treatments of neuromuscular disorders and optimized training of athletes.

Due to its complex interference patterns, decomposition of surface EMG typically requires either processing of large quantities of data [19] or systematic testing of a large number of different MUAP combinations [32]. Both processes can be made fully automatic and can rely on *a priori* knowledge of the EMG mixing process in order to narrow down the space of possible solutions. Nevertheless, both processes require considerable computation power and reported processing times, measured on regular personal computers, ranging from a few seconds [18] to a few minutes [27] per each second of acquired EMG signal. This limits the decomposition of EMG signals to research laboratories and offline analysis.

The need for robust online decomposition of EMG is substantial, not only in the clinical sector that faces everyday lack of time and requires fast diagnostic tools, but also in the field of rehabilitation, sport and ergonomics, where human responses need to be evaluated swiftly and interaction with the environment adapted accordingly. This poses a significant challenge to the aforementioned decomposition techniques as, to the best of our knowledge, no technique for real-time decomposition of EMG has been proposed up to now.

This study presents and validates the real-time version of previously published Convolution Kernel Compensation (CKC) technique [16] and [19]. Modifications of the CKC algorithm to the real-time processing are presented, along with the results of synthetic and experimental surface EMG decomposition. The novel algorithm was tested on experimental surface EMG signals from eight healthy male subjects and its performance was compared to the previously validated batch version of CKC. Finally, computational complexity of real-time CKC is analyzed to verify its suitability for online processing. Part of the results of this study has previously been reported in abstract form in [12] and [13].

II. Data Model

Throughout the manuscript boldface uppercase letters denote matrices, boldface lowercase letters denote vectors and italics

Manuscript received January 30, 2012; revised July 21, 2012 and October 15, 2012; accepted December 16, 2012. Date of publication March 06, 2013; date of current version November 04, 2013. This work was supported by a Marie Curie reintegration grant within the 7th European Community Framework Programme (iMOVE, Contract 239216) and by Grant Agreement ICT-2011.5.1-287739, "NeuroTREMOR: A novel concept for support to diagnosis and remote management of tremor".

V. Glaser is with the Faculty of Electrical Engineering and Computer Science, System Software Laboratory, University of Maribor, Maribor, Slovenia.

A. Holobar and D. Zazula are with the Faculty of Electrical Engineering and Computer Science, University of Maribor, Maribor, Slovenia.

Digital Object Identifier 10.1109/TNSRE.2013.2247631

denote scalars. Discrete time series are denoted by the subscripted boldface lowercase letters, e.g., $\mathbf{x}_i = \{x_i(n); n = 0, 1, \ldots\}$, where $x_i(n)$ denotes a single (the nth) sample. The vector of samples taken from M time series at the nth time instant is denoted by $\mathbf{x}(n) = [x_1(n), \ldots, x_M(n)]^T$. The superscript ^{T} stands for transpose, while $^{-1}$ denotes the matrix inverse. The circumflex $\hat{c}$ denotes an estimate of c.

Multichannel surface EMG acquired during isometric muscle contractions can be modeled as linear shift-invariant convolutive multiple input–multiple output (MIMO) system with M different observations (EMG channels) $\mathbf{x}_i = \{x_i(n); n = 0, 1, 2, \ldots\}; i = 1, \ldots, M$. Each observation comprises contributions from N sources (MUs)

$$x_i(n) = \sum_{j=1}^{N} \sum_{l=0}^{L-1} h_{ij}(l) s_j(n-l), \quad i = 1, \ldots, M \tag{1}$$

where h_{ij} is a L-samples-long MUAP of the jth MU, as it appears in the ith observation, and $s_j(n)$ stands for the nth sample in the train of unit-sample pulses. These pulses denote the discharge times of the jth MU

$$s_j(n) = \sum_{k=-\infty}^{\infty} \delta\left[n - \Psi_j(k)\right], \quad j = 1, \ldots, N \tag{2}$$

where $\delta(.)$ stands for the unit-sample pulse and $\Psi_j(k)$ for the time of the kth discharge of the jth MU. In compact notation, convolution (1) can be written as

$$\mathbf{x}(n) = \mathbf{H}\mathbf{s}(n) \tag{3}$$

where MUAPs from all MUs have been combined into so-called mixing matrix $\mathbf{H}$ [16] and $\mathbf{s}(n) = [s_1(n), s_1(n-1), \ldots, s_1(n-L+1), s_2(n) \ldots . s_N(n-L+1)]^T$ comprises L-samples-long blocks of discharge patterns of all MUs (see [16] for details). Finally, additive colored zero-mean noise $\omega(\mathrm{n})$, typically assumed to be ergodic Gaussian random process, is added to observations

$$y_i(n) = x_i(n) + \omega_i(n); \quad i = 1, \ldots, M. \tag{4}$$

In order to improve the numerical conditioning of the aforementioned mixing model, the derived data model can be extended with $K-1$ delayed repetitions of each observation [16]

$$\overline{\mathbf{y}}(n) = [y_1(n), y_1(n-1), \ldots, y_1(n-K+1), \ldots, y_M(n), y_M(n-1), \ldots, y_M(n-K+1)]^T. \tag{5}$$

We will further assume the correlation matrix of extended observations can be estimated as

$$\widehat{\mathbf{C}}_{\overline{\mathbf{y}}\overline{\mathbf{y}}} = \frac{1}{D} \sum_{n=0}^{D-1} \overline{\mathbf{y}}(n) \overline{\mathbf{y}}^T(n). \tag{6}$$

III. Real-Time CKC Decomposition

CKC blindly estimates discharges $\mathbf{s}_j$ of the jth MU. The method is fully automated, minimally sensitive to the anatomy of investigated muscles and has been validated on experimental signals from various muscles of more than 250 subjects [18], [19] and [26]. The starting point is so-called activity index $\gamma(n)$ [16]

$$\gamma(n) = \overline{\mathbf{y}}(n)^T \widehat{\mathbf{C}}_{\overline{\mathbf{y}}\overline{\mathbf{y}}}^{-1} \overline{\mathbf{y}}(n). \tag{7}$$

In the second step, cross-correlation vector $\mathbf{c}_{\overline{\mathbf{s}}_j, \overline{\mathbf{y}}}$ between $\overline{\mathrm{s}}_j(n)$ and $\overline{\mathbf{y}}(n)$ is blindly estimated [16] and the discharge pattern of the jth MU identified as

$$\hat{s}_j(n) = \hat{\mathbf{c}}_{\overline{\mathbf{s}}_j, \overline{\mathbf{y}}}^{\mathrm{T}} \widehat{\mathbf{C}}_{\overline{\mathbf{y}}\overline{\mathbf{y}}}^{-1} \overline{\mathbf{y}}(n). \tag{8}$$

The real-time version of CKC upgrades the batch CKC technique by reducing the time support for computation of $\widehat{\mathbf{C}}_{\overline{\mathbf{y}}\overline{\mathbf{y}}}$. It updates the matrix values in real time, i.e., when new observation vectors $\mathbf{y}(n)$, or a shorter sequence of these, become available. It also estimates the cross-correlation vector $\hat{\mathbf{c}}_{\overline{\mathbf{s}}_j, \overline{\mathbf{y}}}$ in an iterative manner. The method comprises two main steps: the batch initialization and the online iterative decomposition.

A. Initialization

Denote a block with R samples of observations $\overline{\mathbf{y}}(n), 0 \leq n \leq R-1$, by $\overline{\mathbf{Y}}_R$ and its correlation matrix by $\mathbf{C}_{\overline{\mathbf{Y}}_R \overline{\mathbf{Y}}_R}$. In the initialization part, $\mathbf{C}^{-1}_{\overline{\mathbf{Y}}_R \overline{\mathbf{Y}}_R}$ is computed on the entire block of R samples. Activity index $\gamma(n)$, as defined in (7), is then used to iteratively identify O different time instants $n_{j,\overline{\mathbf{Y}}_R}$ in $\overline{\mathbf{Y}}_R$ with at least one active MU in each time instant

$$n_{j,\overline{\mathbf{Y}}_R} = \max \mathrm{arg}_n \left(\gamma(n)\right), \; j{=}1, \ldots, O, \; n{=}0, \ldots, R-1$$
$$\gamma(n_{j,\overline{\mathbf{Y}}_R}) = 0 \tag{9}$$

where the values of activity index at identified $n_{j,\overline{\mathbf{Y}}_R}$ are set to zero in order to prevent multiple identifications of the same time instant. The number O of time instants $n_{j,\overline{\mathbf{Y}}_R}$ is a parameter and should approximately reflect the number of MUs contributing to $\overline{\mathbf{Y}}_R$. In this study, O was set to 30.

Afterwards, the starting set of cross-correlation vector estimates $\hat{\mathbf{c}}_{\overline{\mathbf{s}}_j, \overline{\mathbf{y}}}$ is initialized as [17]

$$\hat{\mathbf{c}}^T_{\overline{\mathbf{s}}_j, \overline{\mathbf{Y}}_R} = \overline{\mathbf{y}}(n_{j,\overline{\mathbf{Y}}_R}), \quad j = 1, \ldots, O \tag{10}$$

and the first R samples of $s_j(n)$ are estimated as

$$\hat{s}_{j,\overline{\mathbf{Y}}_R}(n) = \hat{\mathbf{c}}^T_{\overline{\mathbf{s}}_j, \overline{\mathbf{Y}}_R} \widehat{\mathbf{C}}^{-1}_{\overline{\mathbf{Y}}_R \overline{\mathbf{Y}}_R} \overline{\mathbf{y}}(n), \quad n = 0, \ldots, R-1 \tag{11}$$

where explicit notations $\hat{\mathbf{c}}_{\overline{\mathbf{s}}_j, \overline{\mathbf{Y}}_R}$ and $\hat{s}_{j,\overline{\mathbf{Y}}_R}(n)$ were used to stress that the cross-correlation vector and the estimate of $s_j(n)$ are calculated from the R-samples-long initialization block of observations $\overline{\mathbf{Y}}_R$.

These estimates are then deployed to update the set of discharges $\widehat{\mathbf{\Psi}}_{j,\overline{\mathbf{Y}}_R}$ for the jth MU by the following threshold operation:

$$\widehat{\mathbf{\Psi}}_{j,\overline{\mathbf{Y}}_R} = \{n | \hat{s}_{j,\overline{\mathbf{Y}}_R}(n) \geq \alpha_{j,\overline{\mathbf{Y}}_R}\}, \quad n = 0, \ldots, R-1 \quad (12)$$

where threshold $\alpha_{j,\overline{\mathbf{Y}}_R}$ is estimated by minimizing the penalty function [17]

$$f(\widehat{\mathbf{\Psi}}_{j,\overline{\mathbf{Y}}_R}) = 100 \cdot \chi_{[6,40]}(G) + CoV_{ISI} \quad (13)$$

with G and $\mathrm{CoV_{ISI}}$ denoting median of discharge rate and the coefficient of variability for interspike intervals in $\widehat{\mathbf{\Psi}}_{j,\overline{\mathbf{Y}}_R}$, respectively. The indicator function $\chi_{[6,40]}(\mathrm{G})$ penalizes MUs with G below 6 pulses per second (pps) or above 40 pps

$$\chi_{[6,40]}(G) = \begin{cases} 0, & \text{if } G \in [6,40] \\ 1, & \text{if } G \notin [6,40] \end{cases}. \quad (14)$$

In order to avoid multiple identifications of the same MU, the estimated discharge times $\widehat{\mathbf{\Psi}}_{j,\overline{\mathbf{Y}}_R}$ are mutually compared and all but the best estimates of each MU, as determined by the penalty function (13), are discarded. This significantly reduces the computational complexity of updates of $\hat{\mathbf{c}}_{\overline{\mathbf{s}}_j,\overline{\mathbf{Y}}_R}$ in the online iterative part of real-time CKC.

B. Iterative Part of CKC

In the iterative part, the Sherman-Morrison-Woodbury formula is employed to iteratively update the inverse of correlation matrix $\mathbf{C}^{-1}_{\overline{\mathbf{Y}}\overline{\mathbf{Y}}}$ for every new block of Q observation samples [12], [29]

$$\widehat{\mathbf{C}}^{-1}_{\overline{\mathbf{Y}}_{D+Q}\overline{\mathbf{Y}}_{D+Q}} = \widehat{\mathbf{C}}^{-1}_{\overline{\mathbf{Y}}_D\overline{\mathbf{Y}}_D} - \widehat{\mathbf{C}}^{-1}_{\overline{\mathbf{Y}}_D\overline{\mathbf{Y}}_D}\overline{\mathbf{Y}}_Q \times \left(\mathbf{I} + \overline{\mathbf{Y}}_Q^T \widehat{\mathbf{C}}^{-1}_{\overline{\mathbf{Y}}_D\overline{\mathbf{Y}}_D}\overline{\mathbf{Y}}_Q\right)^{-1} \overline{\mathbf{Y}}_Q^T \widehat{\mathbf{C}}^{-1}_{\overline{\mathbf{Y}}_D\overline{\mathbf{Y}}_D} \quad (15)$$

where $\widehat{\mathbf{C}}_{\overline{\mathbf{Y}}_D,\overline{\mathbf{Y}}_D}$ is correlation matrix as estimated from previous D samples of $\overline{\mathbf{y}}$, $\overline{\mathbf{Y}}_Q$ represents the block of Q newly arrived samples, and $\mathbf{I}$ stands for matrix identity. Analogously, old samples may be removed from the correlation matrix of observations, keeping only D last samples and, thus, adapting the data model (3) to time-varying mixing matrix $\mathbf{H}$. The value of parameter D depends on the dynamics of the mixing process and is application dependant.

In analogy with the correlation matrix, estimates of cross-correlation vectors $\hat{\mathbf{c}}_{\overline{\mathbf{s}}_j,\overline{\mathbf{Y}}_D}$ have to be updated after each new block of Q samples [13]. First, the pulse train of the jth MU is identified in every new block of samples

$$\hat{s}_{j,\overline{\mathbf{Y}}_{D+Q}}(n) = \begin{cases} \hat{s}_{j,\overline{\mathbf{Y}}_D}(n), & n < D \\ \hat{\mathbf{c}}^{\mathrm{T}}_{\overline{\mathbf{s}}_j,\overline{\mathbf{Y}}_D}\widehat{\mathbf{C}}^{-1}_{\overline{\mathbf{Y}}_{D+Q}\overline{\mathbf{Y}}_{D+Q}}\overline{\mathbf{y}}(n), & D \leq n < D+Q \end{cases}. \quad (16)$$

Afterwards, the discharge times $\widehat{\mathbf{\Psi}}_{j,\overline{\mathbf{Y}}_{D+Q}}$ of the jth MU are computed in the available segment of $D+Q$ samples by iterative application of threshold operation (12)

$$\widehat{\mathbf{\Psi}}_{j,\overline{\mathbf{Y}}_{D+Q}} = \left\{n \middle| \hat{s}_{j,\overline{\mathbf{Y}}_{D+Q}}(n) \geq \alpha_{j,\overline{\mathbf{Y}}_{D+Q}}\right\}, \quad n = 0, \ldots, D+Q-1 \quad (17)$$

with the threshold $\alpha_{j,\overline{\mathbf{Y}}_{D+Q}}$ estimated by the penalty function in (13).

Finally, the cross-correlation vector $\hat{\mathbf{c}}^{\mathrm{T}}_{\overline{\mathbf{s}}_j,\overline{\mathbf{Y}}_D}$ is calculated by averaging observation vectors $\overline{\mathbf{y}}(n)$ over all identified discharges times $\widehat{\mathbf{\Psi}}_{j,\overline{\mathbf{Y}}_{D+Q}}$ in the last $D+Q$ samples

$$\hat{\mathbf{c}}_{\overline{\mathbf{s}}_j,\overline{\mathbf{Y}}_{D+Q}} = \frac{1}{|\widehat{\mathbf{\Psi}}_{j,\overline{\mathbf{Y}}_{D+Q}}|} \sum_{n \in \widehat{\mathbf{\Psi}}_{j,\overline{\mathbf{Y}}_{D+Q}}} \overline{\mathbf{y}}(n) \quad (18)$$

where $|\widehat{\mathbf{\Psi}}_{j,\overline{\mathbf{Y}}_D}|$ is cardinality of $\widehat{\mathbf{\Psi}}_{j,\overline{\mathbf{Y}}_D}$. Note that the definition of $\alpha_{j,\overline{\mathbf{Y}}_{D+Q}}$ requires multiple assessments of the penalty function in (17).

In order to decrease computational complexity, in this study, the penalty function in (13) was assessed at five discrete values, ranging from $\alpha_{j,\overline{\mathbf{Y}}_{D+Q}} = 0.2 \cdot \max(\hat{s}_{j,\overline{\mathbf{Y}}_{D+Q}}(n))$ to $\alpha_{j,\overline{\mathbf{Y}}_{D+Q}} = \max(\hat{s}_{j,\overline{\mathbf{Y}}_{D+Q}}(n))$ in steps of $0.2 \cdot \max(\hat{s}_{j,\overline{\mathbf{Y}}_{D+Q}}(n))$, $n = 0, \ldots, D+Q-1$. A minimum-penalty threshold $\alpha_{j,\overline{\mathbf{Y}}_{D+Q}}$ was selected for further processing.

IV. Signals and Data Analysis

A. Synthetic EMG

Batch CKC and its real-time version were compared on synthetic EMG signals, with the known reference discharge times of simulated MUs. Altogether, five different realizations of a muscle with elliptical cross-section (25 (transversal) × 16 (depth) mm) were simulated using planar volume conductor model [5] and the MU recruitment model [10]. Simulator parameters were similar to those described in [18] and are briefly summarized in the following paragraphs.

The volume conductor comprised an anisotropic semi-infinite muscle layer, 1-mm-thick skin layer, and 3-mm-thick isotropic subcutaneous fat layer. In total, 50 000 simulated muscle fibers were randomly scattered within the muscle cross section, yielding the average muscle fiber density of 200 fibers/mm^2. Average semi-fiber length was 70 mm, with the centers of the innervation zones located 5.0 ± 3.0 mm (normal distribution) distally from the center of the detection system.

A total of 120 MUs with circular territories were randomly distributed within the muscle cross section [2]. Fibers of each MU were interlaced with fibers of many other units. Innervation numbers ranged from 25 to 2500 based on a ∼100-fold range of twitch forces [4]. Normally distributed conduction velocities (4.0 ± 0.3 m/s) were assigned to MUs in the order of their size [4]. Discharge rate of MUs increased linearly from 8 pps at recruitment to 35 pps at maximum voluntary excitation. The last MU was recruited at 80% of maximal excitation. See [10] for detailed description of the employed MU recruitment model.

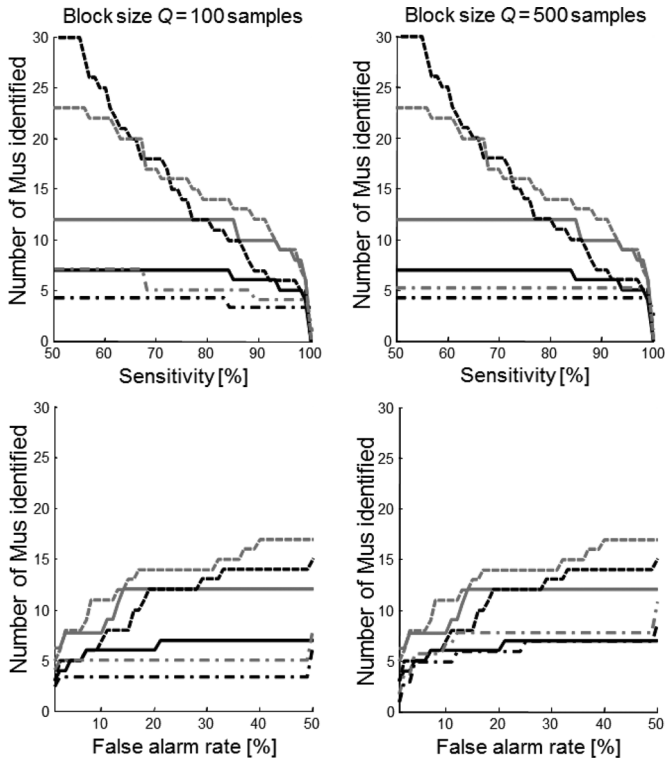

Fig. 1. Cumulative number of identified MUs as a function of sensitivity (upper panels), false alarm rate (lower panels), and size Q of updating block of EMG samples for simulated excitation level of 10% of MVC. Dashed lines stand for LMMSE, solid lines for batch CKC, and dot-dashed lines for real-time CKC. For clarity reasons, only representative results for SNR of 20 dB (gray lines) and 10 dB (black lines) are depicted.

Two different constant excitation levels (10% and 30% of maximum voluntary excitation) were simulated, resulting in 63 and 93 recruited MUs, respectively. The recording system comprised 12 × 5 electrodes of circular shape (radius 1 mm) with 5 mm inter-electrode distance in both directions. A 20-s long longitudinal bipolar signal acquisition was simulated at 2048 samples/s. Finally, zero-mean Gaussian noise, with signal-to-noise ratio (SNR) ranging from 0 to 20 dB (in 5 dB increments) was added to the simulated signals. Representative example of generated surface EMG signal is depicted in Fig. 1.

B. Experimental EMG

Experimental signals were obtained in a controlled environment with the experimental protocol described in [19]. Eight male subjects participated in the experiment. The subjects received a detailed explanation of the study and gave written informed consent prior to participation. The experiments were conducted in accordance with the Declaration of Helsinki and approved by the local ethics committee.

The surface EMG signals were recorded from tibialis anterior muscle during ankle dorsiflexion. The subject was supine on a bed, with the dominant leg placed in an isometric brace for ankle-joint force measurement [19]. The knee was fully extended and the ankle was at 90 degrees. The highest value from three 5-s long measurements of subject's maximum muscle force was used as maximum voluntary contraction (MVC), with 3 min rest between the measurements. After an additional 5 min of rest the subject was asked to perform isometric contraction at 5%, 10%, 15% and 20% of MVC in a randomized order. Two minutes of rest was provided between the measurements.

A detection system was combined from two grids of monopolar electrodes each containing 6 × 5 electrodes with 5 mm interelectrode distance. Each electrode had 2 mm in diameter. The grid was placed on top of innervation zone parallel to muscle fibers. All acquired signals were 20 s long and sampled with 2048 samples/s in 12 bit resolution, amplified with EMG amplifier (LISiN—OT Bioelettronica, Torino, Italy) and bandpass filtered between 10 Hz and 500 Hz.

C. Data Analysis

The simulated and experimental EMG signals were extended by delayed repetitions of each EMG channel with the extension factor in (6) set to $K = 10$. The simulated signals were independently decomposed by real-time CKC, by batch CKC [14], and by linear minimum mean square error (LMMSE) estimator [22]. LMMSE estimator is Bayesian optimal for linear mixing systems and represents the upper performance limit of both CKC methods [14]. Therefore, it was used as a performance reference in this study. However, it assumes the first two moments of source signals, i.e., their mean and their cross-correlation vectors $\hat{\mathbf{c}}_{\overline{\mathbf{s}}_j,\overline{\mathbf{Y}}_R}$, are known in advance and can, thus, be applied only to synthetic signals with known MU discharges. In the case of batch CKC, the number of decomposition runs was set to 30.

Three different performance indices were computed independently for each decomposition technique: the number of identified MUs, the percentage of correctly identified discharges per motor unit, i.e., decomposition sensitivity, and the false alarm rate (percentage of false positives) [19]. Only MUs with sensitivity $\geq$90% and false alarm rate $\leq$10% were considered successfully identified. Discharge time tolerance was set equal to $\pm$0.5 ms [19].

In the case of experimental EMG, real-time CKC was compared to batch CKC only, as LMMSE estimator relies on *a priori* information about MUs that is not available in the experimental data. Furthermore, with the reference discharge patterns of MUs unknown, neither sensitivity nor false alarm rate can be calculated. Thus, the rate-of-agreement between experimentally validated batch CKC [19], [26] and real-time CKC was calculated as

$$RoA_j = \frac{A_j}{A_j + O_{bCKC,j} + O_{rCKC,j}} \tag{19}$$

where A_j denotes the number of discharges of the jth MU identified by both methods (tolerance set to $\pm$0.5 ms), $O_{rCKC,j}$ is the number of discharges identified by real-time CKC only, and $O_{bCKC,j}$ is the number of discharges identified by batch CKC only. When comparing the decomposition results of the two techniques, two MUs were considered commonly identified when they shared at least 30% of all discharges [19].

Finally, the MUAP shapes were estimated by spike triggered averaging of the surface EMG and the estimated MUAP trains

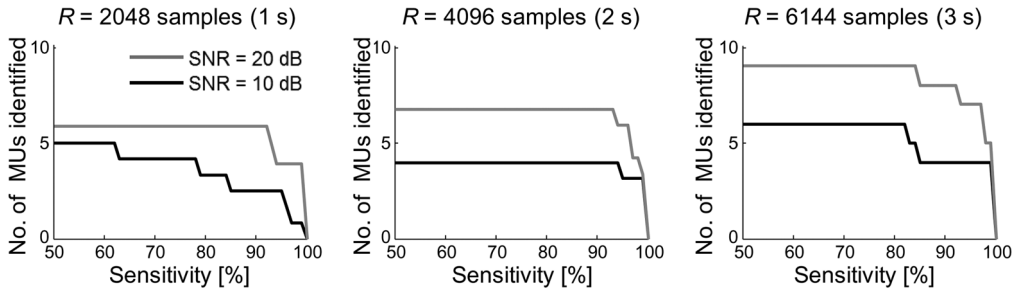

Fig. 2. Cumulative number of MUs identified by real-time CKC decomposition of synthetic surface EMG signals (simulated excitation level of 10% of MVC) as a function of sensitivity and length of initialization block R.

subtracted from the original EMG signals to yield the following signal-to-interference ratio (SIR):

$$\mathrm{SIR}(i) = \left(1 - \frac{E\left[\left(\overline{y}_i(n) - \sum_j z_{ij}(n)\right)^2\right]}{E\left[\overline{y}_i^2(n)\right]}\right) \cdot 100\% \quad (20)$$

where $\overline{\mathbf{y}}_i(n)$ denotes the ith surface EMG channel and $z_i j(n)$ stands for the MUAP train of the jth MU reconstructed from the ith surface EMG signal.

D. Statistical Analysis

The decomposition sensitivity, false alarm rate, and the number of MUs identified by real-time CKC were statistically compared to the results of previously validated batch version of CKC. Because the data was not normally distributed, Wilcoxon signed rank test was used to compare the number of identified MUs (for both synthetic and experimental signals) and paired two-sided signed rank test was used for comparison of sensitivity and false alarm rate of those MUs that were jointly identified by both decomposition techniques (for synthetic signals only). The level of significance was set to $\mathrm{P} < 0.05$.

V. Results

A. Synthetic Surface EMG

Fig. 1 depicts the cumulative number of MUs as a function of: 1) sensitivity and 2) false alarm rates in the estimation of their discharge patterns, averaged over all five simulation runs with excitation level of 10% MVC and the length of updating blocks Q set to 100 and 500 samples, respectively. The length of updating block had no significant impact on the number of identified MUs. Moreover, for the two CKC estimators (but not for LMMSE estimator) the majority of identified MUs had sensitivity in detection of discharges larger than 90%. This robustness in MU identification is not novel and has been previously reported for batch CKC [19].

As demonstrated by results in Fig. 2, the number of MUs identified by real-time CKC depends considerably on the length of initialization block $\overline{\mathbf{Y}}_R$. With longer initialization blocks, real-time CKC provides additional MUs, approaching the performance of batch CKC at the costs of increased decomposition times. Therefore, the length R of the initialization block of EMG signals is application dependent and can be considered a method's parameter.

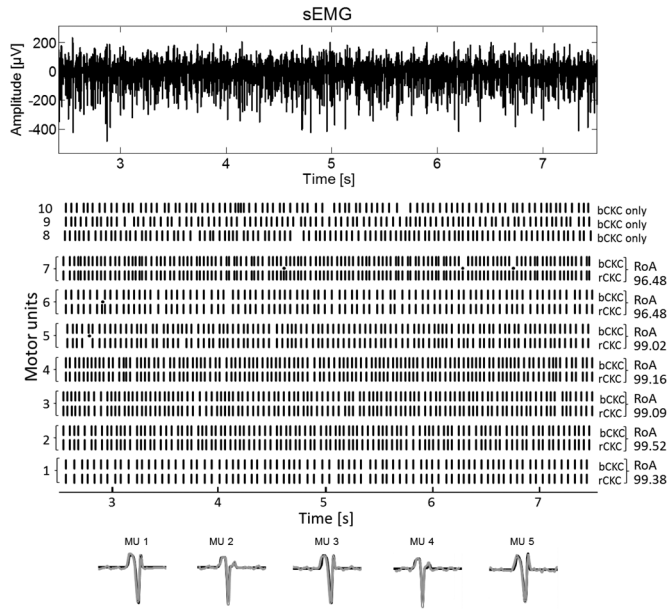

Fig. 3. Representative example of synthetic surface EMG signal with excitation level set to 10% of MVC (upper panel), MU discharge patterns identified by real-time (rCKC) and batch CKC (bCKC) decompositions (central panel), and simulated (black) and estimated (gray) MUAPs (lower panel). Each vertical bar in the central panel represents one MU discharge. Disagreements between the batch and real-time CKC are denoted by small black dots. The initial 2.5 s of the signals were used by the initialization part of real-time CKC. The remaining 17.5 s were processed by the iterative part of real-time CKC. The length of updating block was set to $Q = 250$ samples. The first seven MUs where decomposed by both methods, whereas MU 8, MU 9, and MU 10 were decomposed by batch CKC only. For clarity reasons, only the first 5 s of the MU discharge patterns and one channel of surface EMG are depicted.

Fig. 3 depicts representative examples of MU discharge patterns identified by real-time CKC and batch CKC from synthetic surface EMG with excitation level set to 10% of MVC. Each vertical line represents individual MU discharge, whereas disagreements between both decomposition techniques are denoted by black circles. For real-time CKC, the length of initialization segment was set to $R = 5000$ samples (approximately 2.5 s), whereas the length of updating blocks Q was set to 250 samples. The number of MUs identified from all synthetic EMG signals is summarized in Table I. In the case of 20 dB SNR, 6.6 $\pm$ 1.0 and 4.5 $\pm$ 1.2 MUs were identified in simulations with 10% and 30% excitation level, respectively. In the same signals,

TABLE I
NUMBER OF IDENTIFIED MUS FOR LMMSE, BATCH CKC, AND REAL-TIME CKC (MEAN ±SD) IN THE CASE OF SYNTHETIC SURFACE EMG SIGNALS WITH EXCITATION LEVEL SET TO 10% AND 30% OF MVC, RESPECTIVELY. RESULTS WERE AVERAGED OVER FIVE SIMULATION RUNS. NUMBER OF DECOMPOSITION RUNS OF BATCH CKC WAS LIMITED TO 30. BOTH BATCH CKC AND LMMSE WERE APPLIED TO THE ENTIRE 20 s LONG SIGNALS. FOR REAL-TIME CKC, LENGTH OF INITIALIZATION SEGMENT WAS SET TO $R = 5000$ SAMPLES (APPROXIMATELY 2.5 s), WHEREAS LENGTH OF UPDATING BLOCKS Q WAS SET TO 250 SAMPLES. ALL THE RESULTS OF REAL-TIME CKC ARE SIGNIFICANTLY DIFFERENT FROM RESULTS OF THE LMMSE AND BATCH CKC

excitation level	**10 % MVC**			**30 % MVC**		
SNR	**0 dB**	**10 dB**	**20 dB**	**0 dB**	**10 dB**	**20 dB**
LMMSE	7.0 ± 2.0	9.8 ± 2.1	11.5 ± 1.9	3.5 ± 0.5	6.2 ± 0.5	8.7 ±0.9
batch CKC	3.1 ± 1.3	6.8 ± 1.0	8.7 ± 1.2	2.0 ± 0.5	4.9 ± 0.9	6.0 ± 0.6
real-time CKC	2.1 ± 0.5	4.1 ± 0.6	6.6 ± 1.0	1.5 ± 0.3	3.1 ± 1.0	4.5 ± 1.2

TABLE II
SENSITIVITY (Se) AND FALSE ALARM RATE (Fa) OF MU DISCHARGE PATTERNS THAT WERE SIMULTANEOUSLY IDENTIFIED BY LMMSE, BATCH CKC AND REAL-TIME CKC DECOMPOSITION TECHNIQUES FROM SYNTHETIC SURFACE EMG SIGNALS. RESULTS ARE AVERAGED ACROSS FIVE SIMULATION RUNS AND REPORTED AS MEAN ±SD; * RESULTS OF LMMSE AND BATCH CKC ARE SIGNIFICANTLY DIFFERENT FROM RESULTS OF REAL-TIME CKC ($P < 0.05$)

Simulated excitation level		**10 % MVC**		**30 % MVC**	
SNR	**Method**	**Se [%]**	**Fa [%]**	**Se [%]**	**Fa [%]**
20 dB	**LMMSE**	99.6 ± 0.5*	0.1 ± 0.2	99.7 ± 0.3	0.1 ± 0.2
	batch CKC	99.0 ± 0.6	0.2 ± 0.4	99.7 ± 0.4	0.1 ± 0.4
	real-time CKC	98.7 ± 0.2	0.1 ± 0.3	98.7 ± 1.2	0.1 ± 0.7
10 dB	**LMMSE**	99.8 ± 0.5*	0.2 ± 0.4	99.5 ± 0.4	0.1 ± 0.3
	batch CKC	99.1 ± 0.8	0.3 ± 0.4	98.7 ± 0.9	0.1 ± 0.3
	real-time CKC	98.7 ± 0.1	0.4 ± 0.5	98.6 ± 1.4	0.1 ± 0.4
0 dB	**LMMSE**	99.8 ± 0.2*	0.3 ± 0.3	97.9 ± 1.0	0.3 ± 0.2
	batch CKC	97.8 ± 2.6	0.5 ± 0.4	97.9 ± 1.2	0.3 ± 0.3
	real-time CKC	98.8 ± 2.0	0.5 ± 0.4	97.5 ± 1.1	0.3 ± 0.3

batch version of CKC identified 8.7 ± 1.2 and 6.0 ± 0.6 MUs, and LMMSE 11.5 ± 1.9 and 8.7 ± 0.9 MUs, respectively.

The number of identified MUs decreased with noise. On average, real-time CKC identified 2 MUs with SNR set to 0 dB, whereas batch CKC and LMMSE estimator identified 4 and 7 MUs, respectively. However, both batch CKC and LMMSE operated on the entire 20 s of synthetic EMG signals. In the case of the LMMSE estimator, the discharge patterns of all active MUs were used to train the optimal cross-correlation vectors $\hat{\mathbf{c}}_{\overline{\mathbf{s}}_j,\overline{\mathbf{Y}}_D}$, whereas batch CKC searched the entire 20 s of the signals for plausible initializations of cross-correlation vectors $\hat{\mathbf{c}}_{\overline{\mathbf{s}}_j,\overline{\mathbf{Y}}_D}$. In the real-time CKC, on the other hand, the initialization segment was only 2.5 s long, hindering the identification of all the cross-correlation vectors $\hat{\mathbf{c}}_{\overline{\mathbf{s}}_j,\overline{\mathbf{Y}}_R}$ in the case of severe noise. Nevertheless, the sensitivity in detection of MU discharges was relatively high, as reported in Table II.

B. Experimental EMG Signals

Fig. 4 depicts a representative example of decomposition of experimental surface EMG from tibialis anterior muscle during its isometric contraction at 10% of MVC. Five MUs where decomposed simultaneously by both methods while one additional MU was decomposed by batch CKC. Table III presents the average number of identified MUs, along with the rate-of-agreement between batch and real-time version of CKC, as defined in (19).

The rate-of-agreement between the real-time and batch CKC was relatively low, as only around 83% of MU discharges were identified by both methods. As demonstrated by results in Fig. 4, the majority of decomposition disagreements were located immediately after the initialization phase of real-time CKC (up to

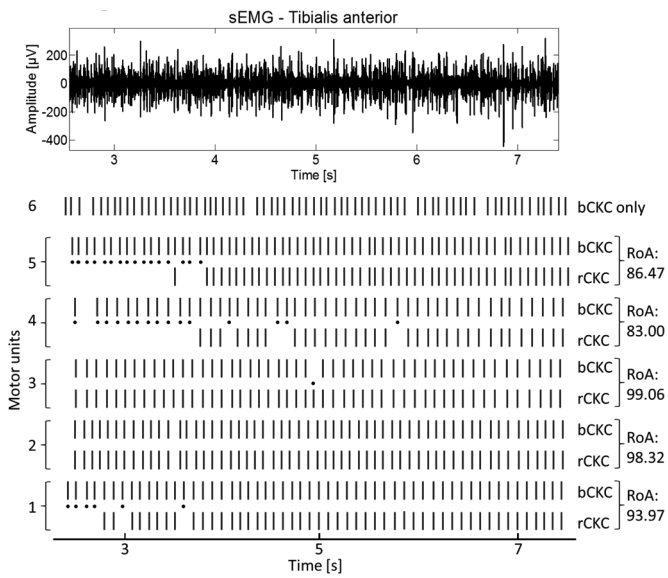

Fig. 4. Representative example of experimental surface EMG signal (upper panel) and MU discharge patterns identified by real-time (rCKC) and batch CKC (bCKC) decompositions of tibialis anterior during its contraction at 10% of MVC (lower panel). Each vertical bar represents one MU discharge. The length of updating block was set to $Q = 250$ samples. The initial 2.5 s of the signals were used by the initialization part of real-time CKC. The remaining 17.5 s were processed by the iterative part of real-time CKC. The first five MUs were decomposed by both methods, whereas MU 6 was decomposed by batch CKC only. Disagreements between the batch and real-time CKC are denoted by small black dots.

TABLE III
NUMBER OF MUS (MEAN ±SD) IDENTIFIED INDEPENDENTLY BY BATCH, BY REAL-TIME CKC AND SIMULTANEOUSLY BY BOTH DECOMPOSITION TECHNIQUES DURING ISOMETRIC CONTRACTIONS OF TIBIALIS ANTERIOR MUSCLE. FOR MUS IDENTIFIED BY BOTH DECOMPOSITION TECHNIQUES THE RATE-OF-AGREEMENT (RoA), AS DEFINED IN (19), IS ALSO REPORTED. RESULTS ARE AVERAGED OVER ALL SUBJECTS; * RESULTS OF REAL-TIME AND BATCH CKC ARE SIGNIFICANTLY DIFFERENT ($P < 0.05$)

Contraction level	No. of MUs (batch CKC)	No. of MUs (real-time CKC)	No. of MUs (both techniques)	RoA [%]
5 % MVC	4.7 ± 1.7*	3.9 ± 1.6*	3.3 ± 0.3	86 ± 17
10 % MVC	4.5 ± 1.4	4.3 ± 1.7	3.5 ± 0.3	83 ± 21
15 % MVC	5.0 ± 1.9	4.5 ± 2.2	3.7 ± 0.4	82 ± 19
20 % MVC	6.0 ± 1.9*	4.5 ± 1.8*	3.7 ± 0.3	82 ± 19

TABLE IV
SIGNAL-TO-INTERFERENCE RATIO (SIR), AS DEFINED IN (20), FOR REAL-TIME AND BATCH CKC APPLIED TO EXPERIMENTAL SURFACE EMG SIGNALS OF TIBIALIS ANTERIOR MUSCLE. RESULTS ARE AVERAGED OVER ALL SUBJECTS. ALL THE RESULTS OF REAL-TIME CKC ARE SIGNIFICANTLY DIFFERENT FROM THE RESULTS OF BATCH CKC

Contraction level	SIR for batch CKC [%]	SIR for real-time CKC [%]
5 % MVC	43.1 ± 5.7	35.5 ± 3.4
10 % MVC	40. 2 ± 3.4	33.8 ± 4.4
15 % MVC	38.9 ± 3.8	28.3 ± 7.9
20 % MVC	35.9 ± 4.9	26.3 ± 9.0

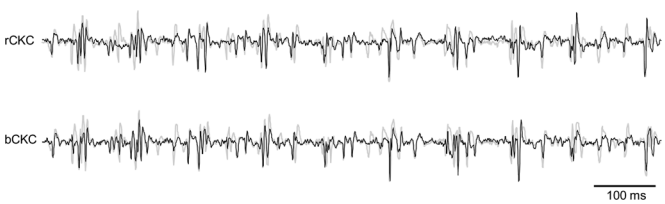

Fig. 5. Surface EMG of the tibialis anterior muscle during its 10% MVC contraction (gray) and the sum of MU action potential trains identified from surface EMG decomposition (black) with real-time CKC (upper plot) and batch CKC (lower plot). For the signals displayed, the signal-to-interference ratio (SIR) was 46% (batch CKC) and 47% (real-time CKC).

the first 4 s of the EMG signals). This was the case for MUs 1, 4 and 5 in Fig. 4, whereas the estimators of MUs 2 and 3 converged already in the initialization part of real-time CKC. When calculated over the last 15 s of the experimental signals (i.e., by allowing the real-time estimators of all MUs to converge), the average rate of agreement between the real-time CKC and batch CKC increased to 90 ± 11%.

The values of SIR, as defined in (20), are summarized in Table IV and exemplified in Fig. 5.

C. Time Complexity

The initialization part of real-time CKC is typically run only once and the number of multiplications and additions required for calculation of matrix $\mathbf{C}^{-1}_{\overline{\mathbf{Y}}_R\overline{\mathbf{Y}}_R}$, activity index $\gamma(n)$ and cross-correlation vector estimates $\hat{\mathbf{c}}_{\overline{\mathbf{s}}_j,\overline{\mathbf{y}}}$ is in the order of $R(KM)^2$. The iterative part of real-time CKC can be divided into two independent processes that run in parallel on multiple core processors. The first process updates the inverse of correlation matrix, whereas the second one updates the cross-correlation vectors $\hat{\mathbf{c}}_{\overline{\mathbf{s}}_j,\overline{\mathbf{Y}}_D}$.

The most time intensive operation is the update of inverse of correlation matrix. Sherman-Morison-Woodbury formula has a cubic complexity [29] and the total number of multiplications and additions per update of inverse of correlation matrix with blocks of Q samples can be estimated as [13]

$$Q^3 + 3\left((KM)^2Q\right) + 2Q^2KM + (KM)^2 + KM \qquad (21)$$

and

$$3(KM)^2Q + 2Q^2KM + KM + Q \qquad (22)$$

respectively, where KM stands for the size of correlation matrix inverse.

Fig. 6 shows the average time used by updates of inverse of correlation matrix and cross-correlation vectors $\hat{\mathbf{c}}_{\overline{\mathbf{s}}_j,\overline{\mathbf{Y}}_D}$ on the Intel Core 2 Quad processor (2.66 GHz, 4 GB of memory) when processing five different realizations of 20-s long synthetic EMG signals with excitation level set to 10% of MVC (initial 2.5 s of the signals were used by the initialization part of real-time CKC). Results were measured for different lengths Q of updating block $\overline{\mathbf{Y}}_Q$, ranging from $Q = 10$ samples up to $Q = 300$ samples. For the block lengths between $Q = 30$ and $Q = 210$ samples, the real-time CKC used less than one second of computation time per each second of recorded surface EMG and can, therefore, be considered a real-time method. With R and Q set to 5000 and 75 samples, respectively, the initialization part of real-time CKC required 0.75 ± 0.06 s, whereas each update in iterative part required additional 0.02 ± 0.06 s. Thus the decomposition of a 20-s long signal was available within 0.02 s after the end of the signal and the real-time CKC required 0.6 s of processing time for every second of acquired multichannel surface EMG. For the same signals, the batch version of CKC required 117 ± 11 s of processing time.

VI. DISCUSSION

Accurate and rapid feedback on neural drive to muscle response is crucial in many fields of neuromuscular research, including neurorehabilitation [14], [3], ergonomics [24], [28], and training of athletes and astronauts [28]. It also represents a fundamental step in investigation of muscle control strategies

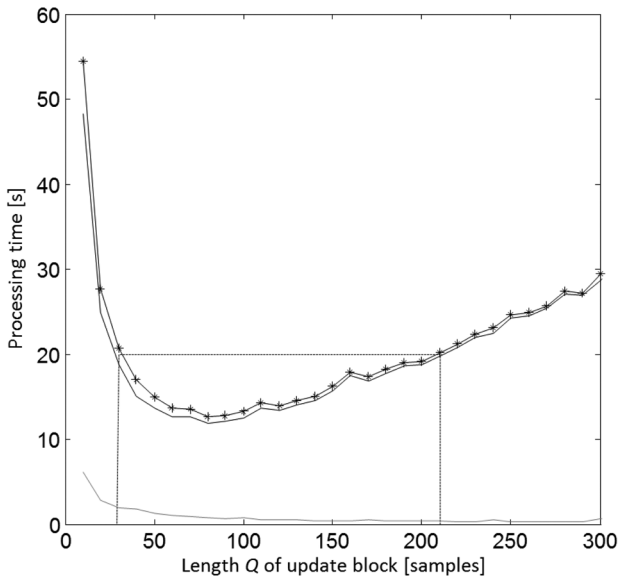

Fig. 6. Average processing time used by iterative part of real-time CKC for calculation of inverse of correlation matrix (solid black line), for updating the ten different cross-correlation vectors (solid gray line), and the sum of both times (black line with asterisks) as a function of length Q of update blocks. Real-time CKC was implemented in Matlab and applied to 20-s long synthetic surface EMG signals. The initial 2.5 s of the signals were used by initialization part of real-time CKC. The remaining 17.5 s were processed by the iterative part of real-time CKC. Results are measured on a personal computer with Intel Core 2 Quad 2.66 GHz processor and 4 GB of memory and averaged over all simulation runs. Correlation matrix of observations was of size of 600×600. For clarity reasons, a dashed rectangle designates the block lengths Q that keep the total processing time of real-time CKC below the EMG signal acquisition time 20 s.

and their plasticity [21]. All aforementioned fields of research typically rely on real-time estimation of surface EMG amplitude that has been demonstrated to be an unreliable indicator of neural drive, mainly due to mutual MUAP cancelation [8]. Different EMG processing steps have been proposed to compensate for EMG amplitude cancellation, including high-pass filtering, rectification, summation and Principal Component Analysis (PCA) of surface EMG signals [36]. However, many of them yielded controversial results and their use is currently under intensive discussion [34]. In this study, a previously introduced and validated CKC decomposition technique [16] has been computationally optimized and algorithmically adapted to real-time online processing. This represents a significant step forward in real-time surface EMG processing, indicating for the first time that the online identification of complete MU discharge patterns is possible during muscle contractions.

The real-time CKC shares the robustness in detection of MU discharges with batch CKC [19]. On average, more than 90% of detected MU discharges were accurately identified from synthetic EMG signals (Table I). Both real-time and batch CKC identified significantly less MUs than asymptotically optimal LMMSE estimator (Table I). However, the required *a priori* knowledge about MU discharges makes the LMMSE estimator useless in practice. It is also noteworthy that, in both real-time and batch CKC, initial searching of possible cross-correlation vectors $\hat{\mathbf{c}}_{\overline{\mathbf{s}}_j,\overline{\mathbf{Y}}_D}$ was deliberately limited to $O = 30$ initial guesses, preferring the processing speed over the number of identified MUs. This also explains why not all MUs identified by real-time CKC have also been identified by batch version of CKC (Table III).

In the case of experimental signals from eight healthy male subjects, fewer MUs were identified by the real-time CKC than by batch CKC, but the differences were not always significant (Table III). Because the LMMSE decomposition is not feasible in this context, batch version of CKC, which has been extensively experimentally validated [18], [19], [26], served as the only reference point. Along with the number of MUs, the SIR, defined in (20), also revealed that the lower portion of energy was identified by real-time CKC than by batch CKC (Table IV). Both methods identified MUs with relatively large contributions to surface EMG, whereas smaller and/or deeper MUs were missed (Fig. 4).

Relatively low initial agreement between the real-time and batch CKC decomposition of experimental signals can be explained by vague initial approximation of cross-correlation vectors $\hat{\mathbf{c}}_{\overline{\mathbf{s}}_j,\overline{\mathbf{Y}}_R}$. Namely, the capability of $\hat{\mathbf{c}}_{\overline{\mathbf{s}}_j,\overline{\mathbf{Y}}_R}$ to separate contributions of different MUs depends on the number of accurately identified MU discharges in the initial block of EMG signal. In the case of experimental signals, estimators of MUs with low number of discharges (or equivalently with low accuracy in identification of MU discharges) in the initialization part required additional few seconds in the iterative part to converge to accurate solutions (Fig. 4). Interestingly, this phenomenon was not evident in the case of synthetic surface EMG signals, illuminating the potential differences between the simulated and experimental conditions.

A crucial feature of real-time CKC is its capability of decomposing high-density surface EMG in real-time. Although relatively fast, the initialization part of real-time CKC produces only coarse estimators of MU discharges, as discussed. The MU estimators are further improved by iterative part of real-time CKC that consists of two computationally intensive, but largely independent processes, the updating of the inverse of correlation matrix of EMG channels and the updating of the cross-correlation vectors $\hat{\mathbf{c}}_{\overline{\mathbf{s}}_j,\overline{\mathbf{Y}}_D}$. Computational complexity of both processes depends on the length of the updating block Q (Fig. 5). For the cross-correlation vectors, the complexity decreases with the length of updating block Q. For the inverse of correlation matrix of EMG channels, the computational complexity exhibits parabolic behavior. The exact location of its minimum depends on the size of the correlation matrix of observations [i.e., on the number of acquired EMG channels and the extension factor K in (6)]. In this study, 60 acquired EMG channels were additionally extended by nine repetitions of each channel, resulting in total of 600 extended EMG channels per contraction. As a result, the minimum of computational complexity was reached at the block length of $Q = 75$ samples. It is also noteworthy that the size of correlation matrix used in this study was typical for CKC-based decomposition (either in batch or real-time mode) and has been experimentally verified on surface EMG signals of more than 250 subjects tested up to now [18], [19] and [26].

The real-time CKC searches for new MUs in the initialization part of the signals only. Therefore, the initialization part of real-time CKC needs to be rerun whenever newly recruited MUs need to be identified. This makes the real-time CKC

method more suited for decomposition of muscle contractions with steady or decreasing MU excitation levels.

In conclusion, the method for real-time decomposition of high-density surface EMG has been introduced and validated. Although consistently identifying fewer MUs than its batch version, real-time CKC shares the robustness in MU identification with batch CKC technique, assuring high accuracy in identification of MU discharges. Its computation complexity depends on the length of the updating blocks of EMG signals, enabling real-time computation on standard personal computers. Although still in validation phase, these results constitute an important contribution to the real-time assessment of neural drive to muscles with potential applications in the field of clinical neurology, neurophysiology, neuromuscular rehabilitation, sports and ergonomics.

REFERENCES

[1] A. Adam and C. J. De Luca, "Recruitment order of motor units in human vastuslateralis muscle is maintained during fatiguing contractions," *J. Neurophysiol.*, vol. 90, no. 5, pp. 2919–2927, 2003.

[2] J. B. Armstrong, P. K. Rose, S. Vanner, G. J. Bakker, and F. J. Richmond, "Compartmentalization of motor units in the cat neck muscle, biventercervicis," *J. Neurophysiol.*, vol. 60, pp. 30–45, 1988.

[3] A. D. Chan and K. B. Englehart, "Continuous myoelectric control for powered prostheses using hidden Markov models," *IEEE Trans. Biomed. Eng.*, vol. 52, no. 1, pp. 121–124, Jan. 2005.

[4] D. Farina, E. Fortunato, and R. Merletti, "Noninvasive estimation of motor unit conduction velocity distribution using linear electrode arrays," *IEEE Trans. Biomed. Eng.*, vol. 47, no. 2, pp. 380–388, Feb. 2000.

[5] D. Farina and R. Merletti, "A novel approach for precise simulation of the EMG signals detected by surface electrodes," *IEEE Trans. Biomed. Eng.*, vol. 48, no. 4, pp. 637–646, Apr. 2001.

[6] D. Farina, K. Yoshida, T. Stieglitz, and K. P. Koch, "Multichannel thin-film electrode for intramuscular electromyographic recordings," *J. Appl. Physiol.*, vol. 104, no. 3, pp. 821–827, 2008.

[7] D. Farina, A. Holobar, M. Gazzoni, D. Zazula, R. Merletti, and R. M. Enoka, "Adjustments differ among low-threshold motor units during intermittent, isometric contractions," *J. Neurophysiol.*, vol. 101, no. 1, pp. 350–359, 2009.

[8] D. Farina, A. Holobar, R. Merletti, and R. M. Enoka, "Decoding the neural drive to muscles from the surface electromyogram," *Clin. Neurophysiol.*, vol. 121, no. 10, pp. 1616–1623, 2010.

[9] C. Farkas, A. Hamilton-Wright, H. Parsaei, and D. W. Stashuk, "A review of clinical quantitative electromyography," *Crit. Rev. Biomed. Eng.*, vol. 38, no. 5, pp. 467–485, 2010.

[10] A. J. Fuglevand, D. A. Winter, and A. E. Patla, "Models of recruitment and rate coding organization in motor unit pools," *J. Neurophysiol.*, vol. 70, pp. 2470–2488, 1993.

[11] M. Gazzoni, D. Farina, and R. Merletti, "A new method for the extraction and classification of single motor unit action potentials from surface EMG signals," *J. Neurosci. Methods*, vol. 136, no. 2, pp. 165–177, 2004, 30.

[12] V. Glaser, A. Holobar, and D. Zazula, "An approach to the real-time surface electromyogram decomposition," in *Proc. 11th Mediterrnanean Conf. Medical and Biological Engineering and Computing*, Ljubljana, Slovenia, 2007, pp. 105–108.

[13] V. Glaser, L. C. Ludeman, A. Holobar, and D. Zazula, "Sequential convolution kernel compensation with block input," in *Proc. 1st WSEAS Int. Conf. Biomedical Electronics and Biomedical Informatics New Aspects of Biomedical Electronics and Biomedical Informatics (BEBI'08)*. Rhodes, Greece: WSEAS Press, Aug. 20–22, 2008, pp. 140–144, cop. 2008.

[14] L. J. Hargrove, E. J. Scheme, K. B. Englehart, and B. S. Hudgins, "Multiple binary classifications via linear discriminant analysis for improved controllability of a powered prosthesis," *IEEE Trans. Neural Syst. Rehabil. Eng.*, vol. 18, no. 1, pp. 49–57, Jan. 2010.

[15] A. Holobar and D. Zazula, "Correlation-based decomposition of surface EMG signals at low contraction forces," *Med. Biol. Eng. Comput.*, vol. 42, pp. 487–496, 2004.

[16] A. Holobar and D. Zazula, "Multichannel blind source separation using convolution kernel compensation," *IEEE Trans. Signal Process.*, vol. 55, no. 11, pp. 4487–4496, Nov. 2007.

[17] A. Holobar and D. Zazula, "On the selection of the cost function for gradient-based decomposition of surface electromyograms," in *Proc. 30th Annu. Int. IEEE EMBS Conf.*, Vancouver, BC, Canada, 2008, pp. 20–24.

[18] A. Holobar, D. Farina, M. Gazzoni, R. Merletti, and D. Zazula, "Estimating motor unit discharge patterns from high-density surface electromyogram," *Clin. Neurophysiol.*, vol. 120, pp. 551–562, 2009.

[19] A. Holobar, M. A. Minetto, A. Botter, F. Negro, and D. Farina, "Experimental analysis of accuracy in the identification of motor unit spike trains from high density surface EMG," *IEEE Trans. Neural Syst. Rehabil. Eng.*, vol. 18, no. 3, pp. 221–229, May 2010.

[20] A. Holobar, V. Glaser, J. A. Gallego, J. L. Dideriksen, and D. Farina, "Noninvasive analysis of motor unit behavior in pathological tremor," in *Conf. Proc. IEEE Eng. Med. Biol. Soc.*, Boston, MA, USA, 2011, vol. 33, pp. 7512–7515.

[21] A. Jackson and E. E. Fetz, "Interfacing with the computational brain," *IEEE Trans. Neural Syst. Rehabil. Eng.*, vol. 19, no. 5, pp. 534–541, Sep. 2011.

[22] S. M. Key, *Fundamentals of Statistical Signal Processing: Estimation theory*. Englewood Cliffs, NJ, USA: Prentice-Hall, 1993, pp. 379–418.

[23] Z. C. Lateva, K. C. McGill, and M. E. Johanson, "The innervation and organization of motor units in a series-fibered human muscle: The brachioradialis," *J. Appl. Physiol.*, vol. 108, no. 6, pp. 1530–1541, 2010.

[24] M. de Looze, T. Bosch, and J. van Dieën, "Manifestations of shoulder fatigue in prolonged activities involving low-force contractions," *Ergonomics*, vol. 52, no. 4, pp. 428–437, 2009.

[25] E. M. Maathuis, J. Drenthen, J. P. van Dijk, G. H. Visser, and J. H. Blok, "Motor unit tracking with high-density surface EMG," *J. Electromyogr. Kinesiol.*, vol. 18, no. 6, pp. 920–930, 2008.

[26] H. R. Marateb, K. C. McGill, A. Holobar, Z. C. Lateva, M. Mansourian, and R. Merletti, "Accuracy assessment of CKC high-density surface EMG decomposition in biceps femoris muscle," *J. Neural Eng.*, vol. 8, no. 6, p. 066002, 2011, [Epub ahead of print].

[27] K. C. McGill, Z. C. Lateva, and H. R. Marateb, "EMGLAB: An interactive EMG decomposition program," *J. Neurosci. Methods*, vol. 149, no. 2, pp. 121–133, 2005, 15.

[28] R. Merletti, A. Botter, C. Cescon, M. A. Minetto, and T. M. Vieira, "Advances in surface EMG: Recent progress in clinical research applications," *Crit. Rev. Biomed. Eng.*, vol. 38, no. 4, pp. 347–379, 2010.

[29] C. D. Meyer, *Matrix Analysis and Applied Linear Algebra*. Philadelphia, PA, USA: SIAM, 2001.

[30] M. A. Minetto, A. Holobar, A. Botter, and D. Farina, "Discharge properties of motor units of the abductor hallucis muscle during cramp contractions," *J. Neurophysiol.*, vol. 102, no. 3, pp. 1890–1901, 2009.

[31] S. H. Nawab, R. P. Wotiz, and C. J. De Luca, "Decomposition of indwelling EMG signals," *J. Appl. Physiol.*, vol. 105, no. 2, pp. 700–710, 2008.

[32] S. H. Nawab, S. S. Chang, and C. J. De Luca, "High-yield decomposition of surface EMG signals," *Clin. Neurophysiol.*, vol. 121, no. 10, pp. 1602–1615, 2010.

[33] F. Negro, A. Holobar, and D. Farina, "Fluctuations in isometric muscle force can be described by one linear projection of low-frequency components of motor unit discharge rates," *J. Physiol.*, vol. 15, no. 587, pt. 24, pp. 5925–5938, 2009.

[34] O. P. Neto and E. A. Christou, "Rectification of the EMG signal impairs the identification of oscillatory input to the muscle," *J. Neurophysiol.*, vol. 103, no. 2, pp. 1093–1103, 2010.

[35] C. Sauvage, M. Manto, A. Adam, R. Roark, P. Jissendi, and C. J. De Luca, "Ordered motor-unit firing behavior in acute cerebellar stroke," *J. Neurophysiol.*, vol. 96, no. 5, pp. 2769–2774, 2006.

[36] D. Staudenmann, K. Roeleveld, D. F. Stegeman, and J. H. van Dieën, "Methodological aspects of SEMG recordings for force estimation—A tutorial and review," *J. Electromyogr. Kinesiol.*, vol. 20, no. 3, pp. 375–387, 2010.

[37] D. Zazula and A. Holobar, "An approach to surface EMG decomposition based on higher-order cumulants," *Comput. Methods Programs Biomed.*, vol. 80, pp. S51–S60, 2005.

Vojko Glaser was born in Maribor, Slovenia, in 1982. He received the B.S. and M.S. degrees in computer science from the University in Maribor, in 2006 and 2010, respectively.

Since 2008, he has been an Assistant at the System Software Laboratory, Faculty of Electrical Engineering and Computer Science, University in Maribor. He assists at lectures regarding system software tools, system administration, logic designs and systems. His research interests include biomedical signal processing and applications. His main research point is measuring and processing of surface EMG signals, EEG and EKG.

Aleš Holobar (M'98) received the B.S. and Ph.D. degrees in computer science from the Faculty of Electrical Engineering and Computer Science (FEECS), University of Maribor (UM), Slovenia, in 2000 and 2004, respectively.

From 2005 to 2008, he was with the Laboratory of Engineering of Neuromuscular System and Motor Rehabilitation, Politechnico di Torino, Italy, with support provided by Italian foundations Cassa di Risparmio di Torino and Institute for Scientific Interchange (from 2005 to 2006), and by a Marie Curie Intra-European Fellowship within the 6th European Community Framework Programme (from 2006 to 2008). Since 2009, he has been an Associate Professor at FEECS, University of Maribor. His research interests include statistical signal processing, compound signal decomposition, identification of multidimensional systems and biomedical imaging, with current activities focused on surface electromyography and biomedical signal processing.

Dr. Holobar is a member of ISEK, IAPR, Slovenian Society of Pattern Recognition and Slovenian Society of Biomedical Engineering.

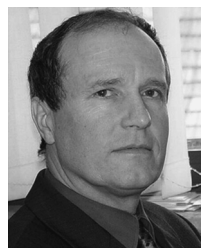

Damjan Zazula (M'87–SM'04) received the Dipl. Ing., Master's, and D.Sc. degrees in electrical engineering from the University of Ljubljana, Slovenia, in 1974, 1978, and 1990, respectively.

After being involved in industrial R&D for 12 years, he joined the Faculty of Electrical Engineering and Computer Science, University of Maribor, Slovenia, in 1987. Currently, he is a Full Professor in computer science, and from 1998 to 2003, he was also appointed an Associate Dean of Research. He has spent several months as a Visiting Professor with the ETH in Zurich, Switzerland, and Ecole Centrale de Nantes, France. His main research interests are compound signal decomposition, biomedical imaging, and virtual training tools.

Dr. Zazula is a member of the IEEE Signal Processing Society, EURASIP, IAPR, Slovenian Technical Society, Slovenian Society of Pattern Recognition, and Slovenian Society of Biomedical Engineering.